Letter

Critical behavior of magnetic polymers on the three-dimensional Sierpiński Gasket

Sumitra Rudra,[1] Damien Paul Foster,[2] and Sanjay Kumar[1]
[1]*Department of Physics, Banaras Hindu University, Varanasi 221 005, India*
[2]*School of Computer Science and Digital Technologies, College of Engineering and Physical Sciences, Aston University, Birmingham BE4 7ET, United Kingdom*

(Received 27 June 2023; accepted 1 September 2023; published 4 October 2023)

We present the (numerically) exact phase diagram of a magnetic polymer on the Sierpińsky gasket embedded in three dimensions using the renormalization group method. We report distinct phases of the magnetic polymer, including paramagnetic swollen, ferromagnetic swollen, paramagnetic collapsed, and ferromagnetic collapsed states. By evaluating critical exponents associated with phase transitions, we located the phase boundaries between different phases. If the model is extended to include a four-site interaction which disfavors configurations with a single spin of a given type, we find a rich variety of critical behaviors. Notably, we uncovered a phenomenon of reentrance, where the system transitions from a collapsed (paramagnetic) state to a swollen (paramagnetic) state followed by another collapse (paramagnetic) and ultimately reaching a ferromagnetic collapsed state. These findings shed new light on the complex behavior of (lattice) magnetic polymers.

DOI: 10.1103/PhysRevE.108.L042502

Magnetic polymers are a new class of functional polymer with magnetic properties, including paramagnetic, ferromagnetic, and ferrimagnetic phases [1,2]. Although they have weaker magnetic properties than cast magnets, they have extensive and diverse applications ranging from material science [3,4], electronics communication [5], acoustic, and optical to biomedical applications including drug delivery [6–9]. A magnetic polymer model of chromosomes has been used to understand how genome organization and epigenetic patterns are linked to each other dynamically [10–13]. Using mean-field theory and Brownian-dynamics simulations, they showed the existence of three possible phases in the steady state and the dynamics of the model generically entails uncontrolled spreading of the dominant epigenetic mark, which is reminiscent of epigenetic silencing dynamics *in vivo*. In spite of its technological importance, the exact phase diagram of a magnetic polymer and the critical exponents associated with various transitions remains elusive.

Thorpe [14] studied q-dependent spin-correlation functions in a model of single magnetic polymer chain using the freely jointed chain model. The model described some of the features of the magnetic polymer but could not describe the influence of excluded-volume effects. Barma [15] considered the excluded volume in presence of the spin-spin correlation function and showed that it is proportional to the generating functions of the probability function describing the spatial distribution of the monomers. Using a mean-field argument, backed up with Monte Carlo simulations, Garel *et al* [16] studied the critical behavior of magnetic polymers in a good solvent where the monomers carry a magnetic moment which interacts ferromagnetically with near-neighbor monomers. Unlike at an ordinary collapse transition, the so called θ point, they observed a strong jump in the polymer density and magnetization. Foster and Majumdar [17] used a flat-PERM approach to observe the first-order character of simultaneous magnetic transition and polymer collapse in three dimensions, but in two dimensions they found that this transition becomes second order. The magnetic polymer has also been studied in three dimensions using the fluctuating bond model [18–22]. Interestingly, the transition was found to be critical and not first order, as in the nonbond fluctuation model [16]. It appears that there is no clear consensus about the phase boundaries between different phases.

Rodrigues and Oliveira recently studied the Ising- and Potts-like magnetic polymers on the Bethe lattice [23]. The Bethe lattice does not allow loops, and therefore corresponds to an extended mean-field-like calculation, which may not capture all the features of the phase diagram. In this context, a hierarchical lattice which allows for loops, along with renormalization group (RG) technique, should provide a good guide to the critical behavior of the model, even if the critical exponents may differ.

In this Letter, we present the results for the Sierpińsky gasket (or four-simplex lattice) in three dimensions, for which the generating function for the polymer chain can be evaluated exactly. By splitting the generating function into a finite subset of partial contributions, it is possible to write a closed set of recursion equations in terms of a finite number of coupling constants. The variables in this set of equations are just the partial generating functions corresponding to different polymer configurations for a given size of the fractal lattice. The recursion relations relate the possible configurations in a block of side ba (as shown in Fig. 1) to equivalent blocks of length a (as shown in Fig. 2), where $b(=2)$ is the scaling factor and a is the distance between nearest-neighbor sites. When applied to the infinite lattice, these recursion relations correspond to an exact real-space renormalization group (RSRG) scheme, providing insights into thermodynamic phases. By varying the initial coupling constants, one can achieve different fixed points corresponding to the various phases and their phase boundaries. Coil-globule transitions [24–26], adsorption transitions [27], mutually attractive and self-avoiding walks of

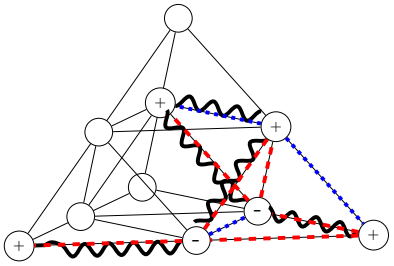

FIG. 1. 3D Sierpińsky gasket with five step walk with nearest-neighbor interactions shown. The walk shown would contribute to A_0 after one step of renormalization (see text).

DNA melting [28,29], and Ising models [30] are some of a few examples which have been solved exactly for the 3D Sierpińsky gasket. At each fixed point, the recursion relations were linearized and the eigenvalues and principal directions calculated. The singular part of the free energy per lattice site is expected to scale near each fixed point as

$$f_{\rm sing} = b^{-d}\tilde{f}(b^{y_1}x_1, b^{y_2}x_2, \cdots),$$

where $\{y_i\}$ is the scaling dimensions and the $\{x_i\}$ are the scaling fields, i.e., how far we are from the fixed point in each eigendirection. The eigenvalues give the distance moved in each iteration, so $\lambda_i = b^{y_i}$ and $y_i = \log(\lambda_i)/\log(b)$. The scaling dimensions are related to correlation-length exponents by $\nu_i = 1/y_i$. The direction i is only relevant if $\lambda_i > 1$.

Here, we consider a self-attracting self-avoiding walk (SASAW) with ferromagnetic spins on the 3D Sierpiński gasket and explore the complete phase diagrams. For this, we introduce an interaction energy $\varepsilon_{nn} < 0$ between nonconsecutive, nearest-neighbor visited sites; each visited site also contains an Ising spin $\sigma_i = \pm 1$. There are Ising-like interactions $\varepsilon_{ij} = -J\sigma_i\sigma_j$ between nearest-neighbor spins σ_i and σ_j. There are no spins on the unvisited sites. The simple model of a magnetic polymer presented here has been studied on the square and cubic lattices [16,17,31], however, the exact phase diagram is not known. By using the exact recursion relations, we obtain the phase diagram on the Sierpińnsky gasket embedded in three dimension. We demonstrate not only the coil-globule transition through temperature or spin-spin interaction variations but also establish the presence

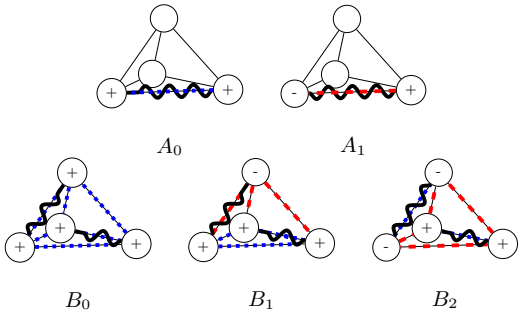

FIG. 2. Figures show the initial weights of the restricted partition functions used in recurrence relations. Wiggly lines corresponds to steps of SAWs. The dotted and dashed lines are interactions between spins of same type and opposite type, respectively.

of swollen and collapsed phases. Both these phases exhibit ferromagnetic and paramagnetic characteristics, with distinct phase boundaries demarcating them. Here, we present a novel scenario involving the existence of three tricritical lines converging at a multicritical point, which segregates three distinct phases.

The restricted partition function, or weights, are shown at first generation in Fig. 2. In this figure we only show the distinct weights; the other weights, which are related by a symmetry operation, are the same (e.g., flipping all the spins together).

The SASAW has been studied on the four-simplex lattice, which is the same as our lattice but where the tetrahedra do not share common sites [24,26]. The recursion relations found by the real-space renormalization group (RSRG) are the same as for the Sierpińsky gasket, but the configurations that can be considered at the first generation are different. In particular, as there are no common sites when the tetrahedron from one generation are assembled to make the next means that the walk is self-avoiding even if it visits multiple sites within one tetrahedron. Adding spins to this model, however, would require more complex recursion relations and would require additional "external" weights at each iteration to take account of all the spin-spin interactions possible. By choosing the Sierpińsky gasket and imposing the self-avoiding condition we must restrict the walk to not take two consecutive steps in the same tetrahedron. This is the same as adding a local rigidity to the walk, which would not be expected to change the critical behavior at large length scales. The model we study is defined by the configurations shown in Fig. 2 with the following initial weights:

$$\begin{aligned} &A_0 = xk, \quad A_1 = xk^{-1}\lambda, \\ &B_0 = x^2y^4k^6, \quad B_1 = x^2y^4\lambda, \quad \text{and } B_2 = x^2y^4k^{-2}, \end{aligned} \tag{1}$$

where $x = \exp(-\beta\mu)$ is the step fugacity, related to the chemical potential μ. $y = \exp(-\beta\varepsilon_{nn})$ is the weight for nearest neighbor interaction, $k = \exp(\beta J)$ is for same type of spins, and $1/k$ is for opposite spins. We have introduced a four-site weight $0 \leqslant \lambda \leqslant 1$ which penalizes single spins of a given type in a given tetrahedron. This extra parameter will enable us to explore the entire phase diagram and the contribution of each fixed point.

The weights include the standard interacting self-avoiding walk in the limit $k \to \infty$ with $x \to 0$ keeping $xk = \kappa$ constant and setting $\lambda = 1$. It is therefore of interest to study the alternative model weights: $\kappa = xk$, $\tau = yk$, and $\alpha = k^{-2}$, which gives the standard SASAW model for $\alpha = 0$ (with all the spins aligned and frozen) and the walk with free spins when $\alpha = 1$, where $x = \kappa$ and $y = \tau$. This gives first generation weights:

$$\begin{aligned} &A_0 = \kappa, \quad A_1 = \alpha\kappa, \\ &B_0 = \kappa^2\tau^4, \quad B_1 = \kappa^2\tau^4\alpha^3, \quad \text{and } B_2 = \kappa^2\tau^4\alpha^4. \end{aligned} \tag{2}$$

The recursion relations are given below. To avoid index overload, we label the generation after n iterations with $\{A_i, B_i\}$, and after $n+1$ iterations with $\{\tilde{A}_i, \tilde{B}_i\}$. The initial

values of $\{A_i, B_i\}$ $(n = 0)$ are determined by the weights x, y, k,

$$\begin{aligned}
\tilde{A}_0 &= \left(A_0^2 + A_1^2\right) + 2\left(A_0^3 + 3A_0A_1^2\right) + 2\left(A_0^4 + 6A_0^2A_1^2 + A_1^4\right) \\
&\quad + 4\big[B_0\left(A_0^3 + A_0A_1^2\right) \\
&\quad + B_1\left(2A_1^3 + 6A_0^2A_1\right) + B_2\left(5A_0A_1^2 + A_0^3\right)\big] \\
&\quad + 6\big[B_0^2A_0^2 + 4A_0A_1B_0B_1 \\
&\quad + 4B_1^2\left(A_0^2 + A_1^2\right) + 2B_0B_2A_1^2 \\
&\quad + 12A_0A_1B_1B_2 + B_2^2\left(3A_0^2 + 2A_1^2\right)\big]; \\
\tilde{A}_1 &= 2A_0A_1 + 2\left(3A_0^2A_1 + A_1^3\right) + 2\left(4A_0^3A_1 + 4A_0A_1^3\right) \\
&\quad + 4\big[B_0A_0^2A_1 + 2B_1A_0^3 + 6B_1A_0A_1^2 \\
&\quad + B_0A_1^3 + 5B_2A_0^2A_1 + B_2A_1^3\big] \\
&\quad + 6\big[2B_0B_1\left(A_0^2 + A_1^2\right) + 4B_0B_2A_0A_1 + 8B_1^2A_0A_1 \\
&\quad + 6B_1B_2\left(A_0^2 + A_1^2\right) + 4B_2^2A_0A_1\big]; \\
\tilde{B}_0 &= \left(A_0^4 + 2A_0^2A_1^2 + A_1^4\right) \\
&\quad + 4\left(B_0A_0^3 + B_1\left(3A_0^2A_1 + A_1^3\right) + 3B_2A_0A_1^2\right) \\
&\quad + 22\big[B_0^4 + 6B_0^2B_1^2 + 12B_0B_1^2B_2 \\
&\quad + 4B_0B_2^3 + 8B_1^4 + 30B_1^2B_2^2 + 3B_2^4\big]; \\
\tilde{B}_1 &= 2\left(A_0^3A_1 + A_0A_1^3\right) \\
&\quad + 3\big[B_0A_0^2A_1 + 3B_1A_0A_1^2 \\
&\quad + B_1A_0^3 + 2B_2A_0^2A_1 + B_2A_1^3\big] \\
&\quad + \left(B_1A_0^3 + 3B_2A_0^2A_1 + 3B_1A_0A_1^2 + B_0A_1^3\right) \\
&\quad + 22\big[B_0^3B_1 + 3B_0^2B_1B_2 + 8B_0B_1^3 \\
&\quad + 15B_0B_1B_2^2 + 24B_1^3B_2 + 13B_1B_2^3\big]; \\
\tilde{B}_2 &= 4A_0^2A_1^2 + 2\big[6B_1A_0^2A_1 + 2B_2A_0^3 + 4B_2A_0A_1^2 \\
&\quad + 2B_1A_1^3 + 2B_0A_0A_1^2\big] \\
&\quad + 22\big[2B_0^2B_1^2 + 2B_0^2B_2^2 + 20B_0B_1^2B_2 \\
&\quad + 4B_0B_2^3 + 8B_1^4 + 26B_1^2B_2^2 + 2B_2^4\big].
\end{aligned}$$

The fixed points were found using multidimensional Newton-Raphson from 10 000 starting points chosen at random in the unit hypercube. This procedure was repeated several times, and we always found the same fixed points. The fixed points of these recursion relations and the corresponding exponents ν are reported in Tables I and II. Once the fixed points are determined and the corresponding eigenvectors $\vec{V}_i$ and values λ_i are calculated, we perturbed each fixed point in each relevant direction. This was done by taking the vector of weights $\vec{W} = (A_i, B_i)$ and adding $\varepsilon\vec{V}_i$ to the weights and iterating. Since, the iteration is discrete, ε needs to be tuned carefully. Too small or large, the iterations will take us to one of the trivial fixed points at 0 or ∞. Suitably tuned, the trajectory passes very close to the target fixed point before diverging. Divergence is inevitable due to rounding errors in the calculations of the eigenvectors. For each direction, we use both $\varepsilon > 0$ and $\varepsilon < 0$. Figure 3 shows the connections between the fixed points. Giving a brief description, the fixed points are: 1, empty lattice; 2, dense ferromagnetic phase; 3, transition between ferromagnetic dense phase and 4/2-paramagnetic dense phase; 4, 4/2-paramagnetic dense phase; 5, dense paramagnetic phase; 6, paramagnetic collapse transition; 7, paramagnetic swollen phase; 8, highest order multicritical point; 9, collapse transition between ferromagnetic swollen phase and 4/2 paramagnetic phase; 10, ferromagnetic collapse transition (θ transition); and 11, the ferromagnetic swollen phase. Whilst we were unable to identify the flows from the high-order multicritical fixed point and the others, this point should occur at the junction of all the phases and transitions, which we will confirm later, and can be seen in Fig. 5 when the extension of the figure to $\lambda \geqslant 0$ is included. The different phases will become apparent below as they appear in the phase diagram. The critical exponents are given in Table II, but the transitions of similar type have the same associated critical exponents (to numerical accuracy), e.g., all the collapse transitions have leading exponents around 0.525 ± 0.005. Fixed points 2–5 correspond to those found for the Ising model on the 3D Sierpińsky gasket [30]. Their weights x, y correspond to ours as follows: $x = B_0/B_2$ and $y = B_1/B_2$ with $A_0 = A_1 = 0$. In their calculation B_2 gives the renormalization of the constant term in the Hamiltonian. Translating into our model, this gives rise to a renormalization

TABLE I. Fixed points found for the recurrence relations.

FP No.	A_0	A_1	B_0	B_1	B_2
1	0.00000	0.00000	0.00000	0.00000	0.00000
2	0.00000	0.00000	0.35688	0.00000	0.00000
3	0.00000	0.00000	0.33723	0.00000	0.11241
4	0.00000	0.00000	0.17844	0.00000	0.17844
5	0.00000	0.00000	0.08922	0.08922	0.08922
6	0.16667	0.16667	0.08333	0.08333	0.08333
7	0.21472	0.21472	0.01250	0.01250	0.01250
8	0.31441	0.00000	0.31677	0.00000	0.10952
9	0.33141	0.00000	0.17921	0.00000	0.16443
10	0.33333	0.00000	0.33333	0.00000	0.00000
11	0.42944	0.00000	0.04998	0.00000	0.00000

TABLE II. Values of correlation length exponents $\nu_i = 1/y_i$ for relevant directions.

FP No.	ν_1	ν_2	ν_3	ν_4	ν_5
1					
2	0.500				
3	0.500	0.553	1.000	∞	
4	0.500	0.500			
5	0.500				
6	0.530	0.867			
7	0.673				
8	0.522	0.570	0.854	1.034	1.154
9	0.523	0.526	0.847	0.865	
10	0.530	0.868	1.062		
11	0.623	0.70			

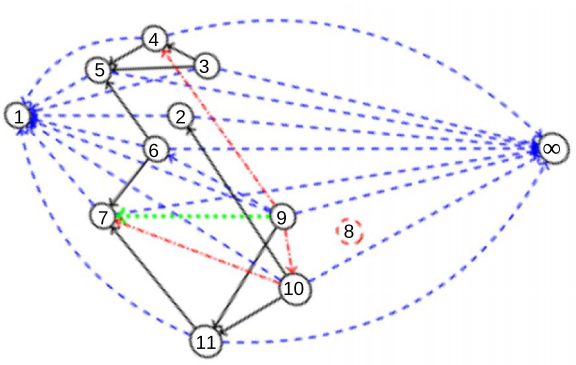

FIG. 3. Schematic fixed point structure. The dashed lines (blue) show the most dominant directions, in most cases to the trivial fixed points (1) and (∞). This direction is the temperaturelike direction. The solid (black) lines give the next most relevant position, the third level is represented by dash dotted (red) lines, and the fourth by a dotted (green) line.

of the fugacity, which needs to be kept distinct in our model. In Ref. [30] they refer to two fixed points at infinity, but here they, and the line between them, collapse to fixed point 3.

It is one thing having the fixed-point structure, but these fixed-points need to be linked to the parameters of the physical model. In order to do this we fix the first generation weights according to the weights given in either Eq. (1) or Eq. (2), depending on the case. We will use Eq. (1) as an example. For fixed interaction weights y and k we tune the fugacity x. The high temperature (low x) phase is determined by the trivial empty lattice fixed point, whilst the low-temperature dense phase is determined by the fixed point at infinity. We tune the fugacity to 14 decimal places and determine the fixed point by the one the iteration was closest to for a significant time. On the whole there is little ambiguity.

We start by confirming the previously studied case of the interacting self-avoiding walk [24]. In order to do this we must take $k \to \infty$ to freeze-out the spins whilst keeping xk finite; this is done by adopting the variables $\kappa = xk$, $\tau = yk$, and $\alpha = 1/k^2$ and setting $\alpha = 0$. The transition line found using the protocol described is shown in Fig. 4(a). The behavior for $\tau < \tau_\theta$ is governed by the fixed point corresponding to a ferromagnetic swollen phase and it is the first relevant

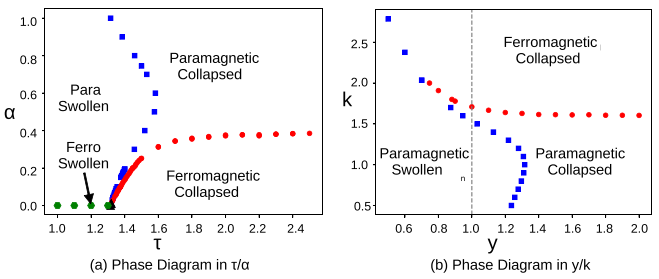

FIG. 4. Phase diagrams are plotted using two equivalent pairs of variables. Triangles and squares represent the ferromagnetic and the paramagnetic θ points, respectively. Hexagons correspond to the ferromagnetic swollen phase and circles to the magnetized dense polymer.

direction which gives the temperature-like behavior, from which we read a correlation length exponent $\nu = 0.623$. For $\tau > \tau_\theta$ the behavior is determined by fixed point which corresponds to a fully ferromagnetic dense phase (only $B_0 \neq 0$). This fixed point only has one relevant direction with a corresponding exponent $\nu = 0.500$, consistent with a discontinuity fixed point as $\nu = 1/d$, where d is the fractal dimension of the lattice, which is in turn consistent with the expected first-order nature of the transition as the fugacity is increased.

Figure 4(a) shows the phase diagram extended to nonzero α. We only observe the ferromagnetic swollen phase when $\alpha = 0$. As soon as $\alpha > 0$, we transition to a paramagnetic swollen phase with a similar value for $\nu = 0.673$. This gives rise to a cross-over exponent for the ferromagnetic line given by $\phi = \nu_1/\nu_2 = 0.623/0.7 \approx 0.89$.

From the fixed-point structure it turns out that the θ ferromagnetic fixed point is connected to the paramagnetic-swollen phase fixed point and not to the corresponding paramagnetic θ point as might have been expected. This means that we should be able to observe a transition from a paramagnetic swollen transition to ferromagnetic collapsed transition via a continuous transition, as seen for the 2D-square lattice [17] for the self-avoiding walk with only Ising-like interactions. Whilst the critical exponent will be the same, the cross-over exponent will be different, with $\phi = \nu_1/\nu_3 = 0.530/1.062 \approx 0.5$ compared to $\phi = \nu_1/\nu_2 = 0.530/0.868 \approx 0.61$ with the standard swollen phase. The line of squares separating the paramagnetic swollen phase from the paramagnetic collapsed phase is a line of paramagnetic tricritical θ like points, with the same first two critical exponents, and so should behave in every way like the usual θ transition for the lattice. The θ point thus extends into a line, now separating the paramagnetic swollen phase from the ferromagnetic collapsed phase. We can see it clearly up to $\alpha = 0.02$ ($k \geqslant 7.1$) and strong evidence that it exists beyond this point. The difficulty is that the paramagnetic collapsed phase enters between the paramagnetic swollen phase and the ferromagnetic collapsed phase, becoming very narrow. It is difficult to locate the precise point where it stops and the line of the θ points start.

Figure 4(b) shows the phase diagram in the standard coordinates. When $y = 1$, there are two transition points: one between the paramagnetic swollen phase and the paramagnetic collapsed phase which is separated by a paramagnetic θ-like transition at $x = 0.160836 \pm 0.000001$, $k = 1.535125 \pm 0.000004$ with the same critical exponents ν and ϕ as the ferromagnetic θ point, but with one less relevant direction in this model. The second transition separates the paramagnetic collapsed phase from the ferromagnetic collapsed phase. The transition point is at $x = 0.120 \pm 0.001$, $k = 1.705 \pm 0.005$. The error bars indicate the region where there is ambiguity over the final fixed point.

We now change λ to allow us to bring into play the other fixed points. Of particular interest is the case $\lambda = 0$, which switches off A_1 and B_1. The phase diagram for this case is shown in Fig. 5(a). Now we can locate exactly the most unstable multicritical point. Setting $\lambda = 0$, we set $A_1 \equiv 0$ and $B_1 \equiv 0$. This then leaves $k = (B_0/B_2)^{1/8} = 1.14197$, $x = A_0/k = 0.255321$, and $y^4 = B_0/(x^2k^6) = 1.884196$ or $y = 1.171605$. In the y-k plane, this point separates three lines. The first,

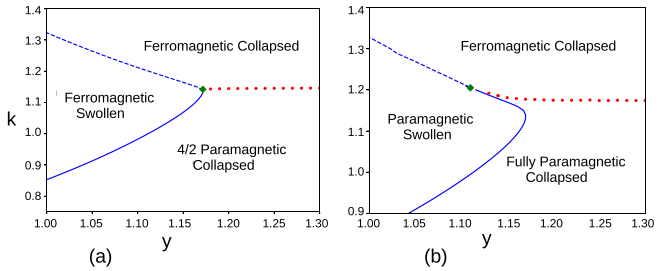

FIG. 5. Phase diagrams with four-spin interactions (a) with $\lambda = 0$ and (b) with $\lambda = 0.01$.

shown as dashed line, is a line of ferromagnetic θ points. The second line, shown as a solid line, is a line of θ-like collapse transitions from the ferromagnetic swollen walk phase to a partially paramagnetic phase which only includes even spin occupancy on the tetrahedron making up the lattice. The third line is a critical line corresponding to the magnetization of the system. The transition is determined by a dense fixed point with $B_0 = 3B_2$ and the other weights zero. The three phases are the ferromagnetic swollen walk phase, the collapsed ferromagnetic phase, and the $4/2$ paramagnetic phase, where $B_1 = 0$ and isolated spins are not allowed.

In Fig. 5(b) the phase diagram is shown when $\lambda = 0.01$. This is small enough to retain some of the features of the $\lambda = 0$ phase diagram, but the phases have changed: the swollen phase has become paramagnetic, and the small k collapsed phase is now fully paramagnetic. What is interesting is that there is still a transition from swollen to ferromagnetic collapsed which is a line of ferromagnetic θ points. There is again a paramagnetic collapsed phase that enters between the paramagnetic swollen and ferromagnetic collapsed phase.

In conclusion we have considered a magnetic polymer model on the 3D Sierpinski gasket employing exact RSRG, exploring its different phases. We introduced a four-spin interaction to explore all fixed points of the model system. Without the four-spin interaction, the system exhibited three distinct phases: the paramagnetic swollen, paramagnetic collapsed, and ferromagnetic collapsed. When the ferromagnetic coupling strength approaches infinity, we recover the standard interacting self-avoiding walk model, with the well-known θ transition. This transition separates a ferromagnetic swollen phases from a ferromagnetic collapsed phase, as expected.

Our extensive analysis of the phase diagrams reveals the presence of a reentrant paramagnetic phase and a transition from the paramagnetic swollen phase to the ferromagnetic collapsed phase, both predominantly governed by the influential θ-point transition. Notably, this reentrant phase occurred from the paramagnetic swollen to the ferromagnetic collapsed phase. Remarkably, this transition was found to be continuous in the 2D realm but exhibited a discontinuous nature in 3D, corroborating the findings of Foster and Debjyoti [17]. As for the Hausdorff dimension of the Sierpinski gasket, it remained consistent with that of the 2D case, standing firmly at $d_H = 2$. Our results for the magnetic walk with solvent interactions on a 2D square and triangular lattice exhibited qualitatively similar patterns, a topic that we intend to explore exhaustively in forthcoming work [32].

An important finding, when the parameter λ was set to zero, was a new phase emerged, namely the partially paramagnetic phase, and a new multicritical point. This identification of a multicritical point with a very rich behavior and regulated by the highest order fixed point added an additional layer of complexity which warrants further studies in our understanding of the magnetic walk preferably with further experiments and simulations. Another surprising result is the paramagnetic swollen phase shows reentrant behavior into the paramagnetic collapsed phase (see Fig. 4). This behavior is tied to the interchange between paramagnetic and ferromagnetic interactions. On the square lattice, the phase diagram exhibits symmetry under $k \to 1/k$, with the ferromagnetic phase mapping onto an antiferromagnetic phase. However, this symmetry is not present in our current context.

Interaction among monomers generally involve dipole interactions. These long-range interactions are screened by the ions in solution, and are effectively short-ranged. When the screening is sufficiently effective, such interactions can be represented by introducing a spin-spin interaction of the form $J_2 S_i^2 S_j^2$, where the three-state spin assumes the value $-1, 0$ and 1.

Financial assistance from the SERB, India; UGC, India; SPARC scheme of MoE; and IoE scheme, MoE, India are gratefully acknowledged.

[1] A. Grein-Iankovski, A. Graillot, M. Radiom, W. Loh, and J.-F. Berret, J. Phys. Chem. C **124**, 26068 (2020).
[2] D. Mostarac, P. A. Sánchez, and S. Kantorovich, Nanoscale **12**, 14298 (2020).
[3] C. Laurvick and B. Singaraju, IEEE Aerosp. Electron. Syst. Mag. **18**, 18 (2003).
[4] D. Romero-Fierro, M. Bustamante-Torres, F. Bravo-Plascencia, A. Esquivel-Lozano, J.-C. Ruiz, and E. Bucio, Polymers **14**, 4084 (2022).
[5] Q. Lu, K. Choi, J.-D. Nam, and H. J. Choi, Polymers **13**, 512 (2021).
[6] K. Mosbach and U. Schröder, FEBS Lett. **102**, 112 (1979).
[7] N. S. Muhazeli, N. A. Nordin, U. Ubaidillah, S. A. Mazlan, S. A. A. Aziz, N. Nazmi, and I. Yahya, Materials **13**, 5637 (2020).
[8] V. T. Tran, D. K. Lee, J. Kim, K.-J. Jeong, C.-S. Kim, and J. Lee, ACS Appl. Mater. Interfaces **12**, 16584 (2020).
[9] M. Swietek, W. Tokarz, J. Tarasiuk, S. Wronski, and M. Blazewicz, Acta Phys. Pol. A **125**, 891 (2014).
[10] D. Colì, E. Orlandini, D. Michieletto, and D. Marenduzzo, Phys. Rev. E **100**, 052410 (2019).
[11] D. Michieletto, E. Orlandini, and D. Marenduzzo, Phys. Rev. X **6**, 041047 (2016).
[12] D. Michieletto, E. Orlandini, and D. Marenduzzo, Sci. Rep. **7**, 14642 (2017).

[13] D. Michieletto, D. Colì, D. Marenduzzo, and E. Orlandini, Phys. Rev. Lett. **123**, 228101 (2019).
[14] M. F. Thorpe, Phys. Rev. B **13**, 2186 (1976).
[15] M. Barma, Phys. Rev. B **18**, 6398 (1978).
[16] T. Garel, H. Orland, and E. Orlandini, Eur. Phys. J. B **12**, 261 (1999).
[17] D. P. Foster and D. Majumdar, Phys. Rev. E **104**, 024122 (2021).
[18] J.-H. Huang and M.-B. Luo, Polymer **45**, 2863 (2004).
[19] J.-H. Huang, M.-B. Luo, and C.-J. Qian, J. Appl. Polym. Sci. **99**, 969 (2006).
[20] M.-B. Luo, Int. J. Mod. Phys. B **17**, 4267 (2003).
[21] M.-B. Luo, J. Chem. Phys. **124**, 034903 (2006).
[22] M.-B. Luo and J.-H. Huang, J. Chem. Phys. **119**, 2439 (2003).
[23] N. T. Rodrigues and T. J. Oliveira, Phys. Rev. E **106**, 024130 (2022).
[24] D. Dhar and J. Vannimenus, J. Phys. A: Math. Gen. **20**, 199 (1987).
[25] S. Kumar and Y. Singh, Phys. Rev. A **42**, 7151 (1990).
[26] G. F. Tuthill and W. A. Schwalm, Phys. Rev. B **46**, 13722 (1992).
[27] S. Kumar, Y. Singh, and D. Dhar, J. Phys. A: Math. Gen. **26**, 4835 (1993).
[28] S. Kumar and D. Giri, J. Chem. Phys. **125**, 044905 (2006).
[29] S. Kumar and Y. Singh, J. Stat. Phys. **89**, 981 (1997).
[30] T. A. Larsson, J. Phys. A: Math. Gen. **18**, L149 (1985).
[31] K. Faizullina and E. Burovski, J. Phys.: Conf. Ser. **1740**, 012014 (2021).
[32] R. Sumitra, D. P. Foster, and S. Kumar (Unpublished).